Next Nanotechnology 10 (2026) 100600

Contents lists available at ScienceDirect

Next Nanotechnology

journal homepage: www.sciencedirect.com/journal/next-nanotechnology

Research Article

Investigation of thermal radiation and chemical reaction impacts on Carreau-Casson nanofluid flow across a stretching sheet: A solar aircraft application

Kandavkovi Mallikarjuna Nihaal [a], Ulavathi Shettar Mahabaleshwar [a,*], Andy Chan [b], Mukannan Arivanandhan [c], Gadigeppa Myacher Sachin [a], Laura Milena Pérez [d]

[a] Department of Studies in Mathematics, Davangere University, Shivagangothri, Davangere 577007, India
[b] Southampton Solent University, East Park Terrace, Southampton SO14 0YN, United Kingdom
[c] Centre for Nanoscience and Technology, Anna University, Chennai 600025, India
[d] Departamento de Ingeniería Industrial y de Sistemas, Universidad de Tarapacá, Casilla 7D, Arica 1000000, Chile

ARTICLE INFO

Keywords:
Nanofluid
Carreau fluid
Stretching sheet
Porous medium
Quadratic thermal radiation
Thermophoresis and brownian motion

ABSTRACT

New advances in nanotechnology are setting up new potential for energy conversion and temperature management, which has significantly improved solar aircraft performance. Considering this application, the present work investigates the impact of quadratic radiation on Carreau-Casson nanofluid across a porous stretched sheet in the presence/absence of slip condition. The governing equations that capture the entire variety of these effects result in highly sophisticated partial differential equations and then the bvp-4c numerical approach is utilized to resolve difficult boundary value problems. The consequences of the various factors over respective profiles concerning the problem are analyzed and displayed visually. The current study's main outcomes reveal that larger values of Weissenberg number, Casson, and porosity decrease fluid flow velocity. Improved temperature profile was achieved for elevated values of radiation, Brownian and Thermophoretic parameters. Further, concentration profile drops for increasing values of Thermophoresis. The quantitative results reveal 7.84% rise in skin friction for growing porosity parameter while larger casson and Weissenberg number cut it to 7.24% and 7.53% with less impact on heat and mass transfer rates. On the hand, upsurge values of brownian and thermophoretic parameter improves heat transfer to 7.56% and 2.36% respectively whereas thermal radiation restrains heat and mass transfer to −0.17% and −0.24% respectively. Also, we have obtained an optimal correlation when we compare the present findings to the previously reported outcomes.

1. Introduction

Nanotechnology is concerned with the development and application of materials at the nanoscale, as well as the integration of the resultant nanostructures into larger systems. Higher relative surface area and quantum implications, which substantially modify or improve qualities such as thermal, electrical, and magnetic behaviour, reactivity, and strength, are the two primary variables influencing nanoscale material behaviour. Nanofluids have various distinguishing characteristics that set them apart from micro or other large-particle dispersions. It has been found that nanofluids have a higher thermal conductivity than traditional cooling fluids such as ethylene glycol, water, and kerosene. The concept of nanofluids was an innovative idea proposed by Choi and Eastman [1]. In their article, they discussed the potential benefits of fluids immersed with nanoparticles. Buongiorno [2] proposed an article about convective transport in nanofluids. The study findings indicate that nanofluids have superior single phase heat transmission coefficients and thermal conductivity compared to traditional fluids. In many studies [3–5] nanofluids have proven to be more significant than other fluids.

Carreau fluid model offers a more comprehensive and accurate evaluation of complicated non-Newtonian fluid behaviour and if often used to simulate the flow behaviour of a range of complex, non-Newtonian fluids, particularly in porous media and industrial applications, than simpler Newtonian or power-law models. Its versatility and ability to identify shear-thinning effects are key advantages for

* Corresponding author.
E-mail addresses: nihaal.kmdvg@gmail.com (K.M. Nihaal), u.s.m@davangereuniversity.ac.in (U.S. Mahabaleshwar), andy.chan@solent.ac.uk (A. Chan), marivucz@annauniv.edu (M. Arivanandhan), sgmwithusm@gmail.com (G.M. Sachin), lperez@academicos.uta.cl (L.M. Pérez).

https://doi.org/10.1016/j.nxnano.2026.100600
Received 1 June 2026; Received in revised form 25 June 2026; Accepted 4 July 2026
Available online 11 July 2026
2949-8295/© 2026 The Author(s). Published by Elsevier Ltd. This is an open access article under the CC BY license (http://creativecommons.org/licenses/by/4.0/).

Nomenclature

A_1, A_2, A_3, A_4 Constants.
C_w Concentration at surface $(molm^{-3})$
C_∞ Concentration at far field $(molm^{-3})$
Cp Specific heat $(Jkg^{-1}K^{-1})$
Cf Skin friction
D_B Brownian parameter (m^2s^{-1})
k^* Permeability (m^2)
k Thermal conductivity $(Wm^{-1}K^{-1})$
K_c chemical reaction parameter (s^{-1})
K Porosity parameter
m Power index number
Nt Thermophoresis parameter

Greek symbols
β Casson parameter
μ Dynamic viscosity $(kgm^{-1}s^{-1})$
υ kinematic viscosity (m^2s^{-1})
σ^* Stefan Boltzmann's constant
θ_p Temperature ratio parameter
φ Solid volume fraction

Abbreviations
ODEs Ordinary Differential Equations
RQTR Rosseland Quadratic Thermal Radiation
PTSCs Parabolic Trough Surface Collectors
Nb Brownian motion parameter
Nu Nusselt number
$\widehat{T}_w$ Wall temperature (K)
$\widehat{T}_\infty$ Temperature at far field (K)
q_w Wall heat flux
q_m Wall mass flux
R Quadratic thermal radiation
Sh Sherwood number
$(\widehat{u}, \widehat{v})$ Velocity components (ms^{-1})
(x, y) Coordinate axes (m)
We Weissenberg number
ρ Density (kgm^{-3})
τ Effective heat capacity ratio
α^* Mean absorption coefficient (m^{-1})
Γ Time constant
(γ, δ) First order and second order slip parameter
η Similarity variable
PDEs Partial Differential Equations
MHD Magnetohydrodynamics

improving industrial processes and understanding the dynamics of complex fluids. Khan et al. [6] investigated MHD fluid flow on a stretched sheet comprising Carreau nanofluid. Entropy generation was investigated to gain a better understanding of irreversibility, heat transport, system optimization, and thermodynamic behavior of fluid system. Santoshi et al. [7] conducted a computational investigation of the three-dimensional Casson and Carreau nanofluid flow. The findings have been obtained for the Casson and Carreau nanofluids. Carreau nanofluid has been discovered to have a faster rate of mass transfer. Li et al. [8] investigated bioconvective flow by adopting Carreau nano liquid over a stretched sheet with a convective boundary. The heat transfer was investigated by employing the CC heat flux and radiation. The use of Carreau nanoparticles was crucial due to their ability to enhance heat and mass transfer. Many studies on Carreau nanofluid with external effects like MHD, activation energy, and CC-heat flux have been published recently [9–11].

Stretching sheet problems have inspired a significant amount of research interest in fluid mechanics and heat transfer. The study of fluid flow and heat transmission over a stretched sheet is vital in numerous industrial fields, including polymer extrusion, glass fibre manufacture, and metal and plastic sheet fabrication. When a fluid is propelled by a moving surface, it builds a boundary layer, resulting in heat and mass transfer processes to take place. Manigandan et al. [12] investigated hybrid nanofluid flow on an exponential stretching surface under the influence of viscous dissipation and activation energy. Using a C-C heat flux model, Nihaal et al. [13] examined how an induced magnetic field affected the flow of ternary nanofluid past a stretched surface. It has been discovered that the fluid flow rises in proportion to the stretching rate. Gamaoun et al. [14] studied the influence of thermal radiation and varying nano liquid density on an electrically conducting flow over a stretched sheet. Zubi et al. [15] explored the influence of Darcy Forchhiemer over second grade nanofluid flow across a bended stretching sheet. Waseem et al. [16] analysed the impact of heat source and radiation on nanofluid flow across a three dimensional stretching surface using OHAM method.

The bigger surface area of a porous media permits better contact between the fluid and the solid material, which can improve processes like heat transmission, distribution of mass, and chemical interactions. Many researchers studied characteristics of heat and mass transfer through the porous media, and their findings may be found in these articles [17–20].

The inclusion of thermal radiation into fluid flow and heat transfer research has yielded fresh insights into thermal process optimization and system design where heat transport is an important issue. Waseem et al. [21] investigated the impact of radiation on hybrid nanofluid flow across a 3D extending surface with entropy generation. The results reveal that entropy rises for increasing values of radiation. Sohail et al. [22] examined the radiation and viscous dissipation impacts on hybrid nanofluid flow among spinning parallel disk. It has been found that radiative heat transmission, particularly quadratic, has a significant impact on fluid dynamics and heat transfer when compared to many other circumstances. Thriveni and Mahanthesh [23] used the response surface technique and studied the KVL model for the quadratic convective flow of hybrid nanofluid flow via micro-annulus. Furthermore, sensitivity analysis was performed to improve the heat transfer rate using quadratic thermal radiation, variable thermal conductivity, and total volume percent of nanoparticles. Rana and Kumar [24] investigated the quadratic form of radiation in the analysis of hybrid nanofluid flow across rotating cylinder. Furthermore, the sensitivity analysis revealed an affirmative linear correlation between the heat transfer rate and the radiation parameter. Influence and findings of quadratic thermal radiation on different fluid flows over stretching surface can be found in these articles [25–27].

The combined impacts of Brownian motion and thermophoresis in the research field of nanofluids have lately received a lot of interest. Abbas and Sohail [28] studied radioactive double diffusion over 3D stretching sheet flow under the influence of thermophoresis and Brownian motion. Hazarika and Ahmed [29] examined thermophoretic and Brownian effect on micropolar nanofluid flow. The synergistic effects of these parameters have a major impact on the behavior of momentum, thermal, and concentration boundary layers, altering fluid flow attributes such as heat and mass transport rates. Sudarmozhi et al. [30] investigated Maxwell fluid in the presence of activation energy, thermophoresis, and Brownian motion over a stretching surface. The study's major findings reveal that Brownian motion plays a vital part in particle transport and dispersion in Maxwell fluid flow across a surface. The

Maxwell fluid flow over a stretching permeable surface with stagnation point in the presence of MHD was studied by Agunbiade et al. [31] under the influence of Thermophoresis and Brownian motion. The comparison of the novel work with the surveyed pre-existing literature is displayed in Table 1.

Reviewing the literature, it is clear that prior research has not properly studied the combined influence of multiple complicated factors on Carreau-Casson nanofluid flow across a stretched sheet. Some of these variables include porous medium, quadratic thermal radiation, thermophoresis, and Brownian motion. The drive for more assessment provides an exciting idea for our present research. The major purpose of this study is to fill the knowledge void by conducting a detailed examination of the complex interaction of these various parameters and their impact on improving heat transfer in solar aircraft. The solar airplane is seen in Fig. 1.

Solar craft wings employ parabolic trough surface collectors (PTSCs) that absorb solar thermal energy while disseminating solar radiation. Solar-powered aircraft research has sparked a lot of attention in recent years as a viable option for long-duration flight. The wing is an important component of these aircraft since it can gather solar energy and enable better flight. Furthermore, the wing design must enhance the aircraft's aerodynamic performance to maximize lift-to-drag ratio and reduce energy use. In this study, heat transfer on solar aircraft utilizing nanofluid has been theoretically explored. The demonstration in Fig. 2 is intended to show the solar-powered airplane wing with a parabolic-shaped reflective trough.

2. Mathematical modeling

This study examines the flow of two dimensional Carreau Casson nanofluid via porous extended surface in the presence of chemical reaction. The Carreau fluid is then dispersed with a nanofluid containing nanoparticle *Go* and conventional fluid, such as sodium alginate. The surface is stretching along x axis with velocity $u_w(x) = ax$ and perpendicular to y axis (see Fig. 3). The sheet exchanges heat with quadratic thermal radiation hence the sheet's temperature is assumed to be $\widehat{T}_w$ and outside the thermal boundary as $\widehat{T}_\infty$. The optimization of heat and mass transfer is studied using Thermophoresis and Brownian motion, and chemical reaction that produces concentration gradients influencing overall kinetics and mass transfer resistance. The rheological model for an isotropic and incompressible flow of Casson fluid is considered as follows (see [30]):

$$\tau = 2e_{ij}\left(\mu_b + \frac{p_y}{\sqrt{2\pi}}\right),\ \pi > \pi_c,\ \tau = 2e_{ij}\left(\mu_b + \frac{p_y}{\sqrt{2\pi_c}}\right),\ \pi < \pi_c. \tag{1}$$

.

In the context of Casson modelling, the constant π indicates product of deformation rate component and factor π_c indicates a considerable assessment of π.

Table 1
The current research comparison with previous studies.

Work	Ali [32]	Ramzan [33]	Jyothi [34]	Present study
Carreau-Casson fluid	✓	✓	✓	✓
Porous Medium	✓	✓	×	✓
Quadratic thermal radiation	×	×	×	✓
Thermophoresis, Brownian motion	×	✓	✓	✓
Chemical Reaction	×	✓	✓	✓
Stretched sheet	✓	×	×	✓
Fluid type				
Mono	×	×	✓	✓
Hybrid	×	✓	×	×
Ternary	✓	×	×	×

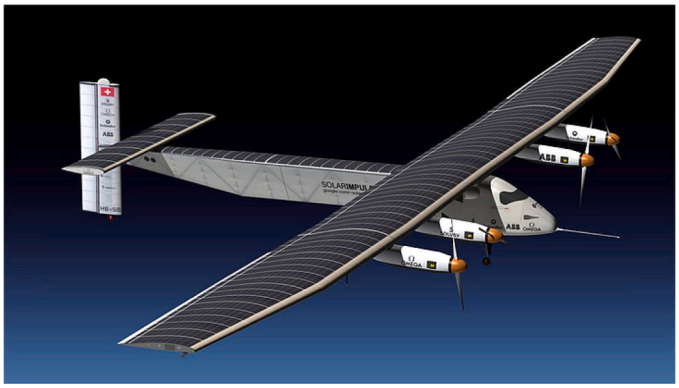


Fig. 1. Solar aircraft.

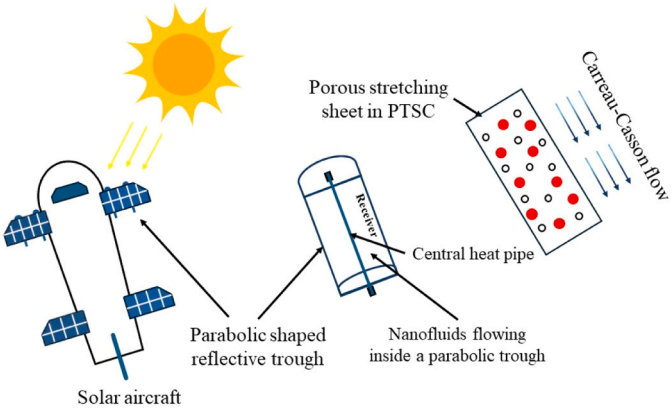


Fig. 2. A pictorial description of the current study.

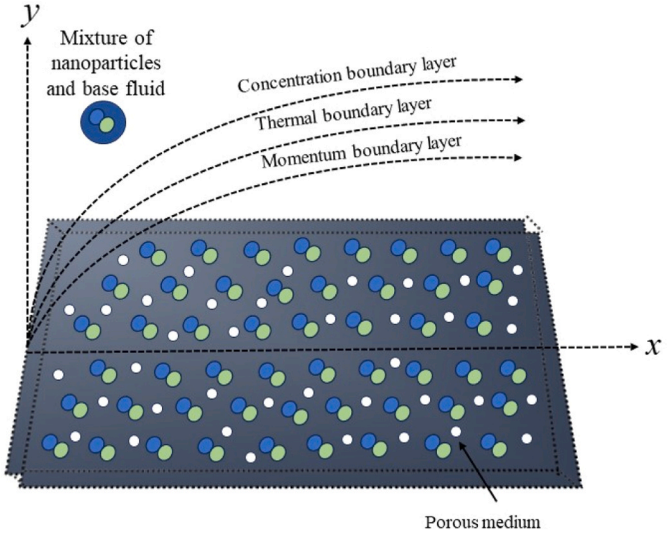


Fig. 3. Illustration of the flow problem.

In the context of Rosseland approximation, the heat flux is given as follows:

$$q_r = -\frac{4}{3\alpha^*}\nabla(e_b),\ e_b = \sigma^*\widehat{T}^4. \tag{2}$$

.

Higher-order relations are not looked at if the temperature fluctua-

tion in the flow allows for extending $\widehat{T}^4$ in a Taylor series near to $\widehat{T}_\infty$. Then we have,

$$\widehat{T}^4 \approx 3\widehat{T}_\infty^4 - 8\widehat{T}_\infty^3\widehat{T} + 6\widehat{T}_\infty^2\widehat{T}^2 .... \tag{3}$$

.

Based on above considerations, the governing flow equations are derived as follows see ([32,35–38]),

$$\frac{\partial\widehat{u}}{\partial x} + \frac{\partial\widehat{v}}{\partial y} = 0, \tag{4}$$

$$\widehat{u}\frac{\partial\widehat{u}}{\partial x} + \widehat{v}\frac{\partial\widehat{u}}{\partial y} = \upsilon_{nf}\left(\left\{1+\frac{1}{\beta}\right\} + \left\{1+\Gamma^2\frac{\partial\widehat{u}}{\partial y}^2\right\}^{(m-1)/2}\right)\frac{\partial^2\widehat{u}}{\partial y^2} - \frac{\upsilon_{nf}}{k^*}\widehat{u} \\ \upsilon_{nf}(m-1)\Gamma^2\frac{\partial^2\widehat{u}}{\partial y^2}\frac{\partial\widehat{u}}{\partial y}^2\left\{1+\Gamma^2\frac{\partial\widehat{u}}{\partial y}^2\right\}^{(m-3)/2} \tag{5}$$

$$\widehat{u}\frac{\partial\widehat{T}}{\partial x} + \widehat{v}\frac{\partial\widehat{T}}{\partial y} = \frac{1}{(\rho Cp)_{nf}}\left(k_{nf}\frac{\partial^2\widehat{T}}{\partial y^2} - \frac{\partial q_r}{\partial y}\right) + \tau\left\{D_B\frac{\partial\widehat{C}}{\partial y}\frac{\partial\widehat{T}}{\partial y} + \frac{D_{\widehat{T}}}{\widehat{T}_\infty}\left(\frac{\partial\widehat{T}}{\partial y}\right)^2\right\} \tag{6}$$

$$\widehat{u}\frac{\partial\widehat{C}}{\partial x} + \widehat{v}\frac{\partial\widehat{C}}{\partial y} = D_B\frac{\partial^2\widehat{C}}{\partial y^2} + \frac{D_{\widehat{T}}}{\widehat{T}_\infty}\frac{\partial^2\widehat{T}}{\partial y^2} - K_r^*(C-C_\infty) \tag{7}$$

and boundary conditions [39]

$$\widehat{u} = \widehat{u}_w + \left(1+\frac{1}{\beta}\right)U_{slip},\ \widehat{v} = 0,\ \widehat{T} = \widehat{T}_w,\ \widehat{C} = \widehat{C}_w,\ \text{at } y = 0, \tag{8}$$

$$\widehat{u}\to 0,\ \widehat{T}\to\widehat{T}_\infty,\ \widehat{C}\to\widehat{C}_\infty \tag{9}$$

.

Here, $(\widehat{u}, \widehat{v})$ represents velocity constraints along (x, y) axis respectively. β represents Casson parameter, Γ represents time constant, power law index is denoted by m, k^* and ρ denotes permeability and density respectively. (μ, υ) are the dynamic and kinematic viscosity, k is the thermal conductivity, σ^* refers to Stefan-Boltzmann's constant, α^*-Rosseland mean absorption coefficient and $U_{slip} = Au_{yy} + Bu_{yy}$, where, A and B are considered to be constant.

With the help of Eqs. (2) and (3), the energy Eq. (6) comprising Rosseland quadratic thermal radiation (RQTR) becomes:

$$\widehat{u}\frac{\partial\widehat{T}}{\partial x} + \widehat{v}\frac{\partial\widehat{T}}{\partial y} = \frac{1}{(\rho Cp)_{nf}}\left(k_{nf} - \frac{32\sigma^*\widehat{T}_\infty^3}{3\alpha^*}\right)\frac{\partial^2\widehat{T}}{\partial y^2} + \frac{24\sigma^*\widehat{T}_\infty^3}{3\alpha^*}\frac{\partial^2(\widehat{T}^2)}{\partial y^2} \\ +\tau\left\{D_B\frac{\partial\widehat{C}}{\partial y}\frac{\partial\widehat{T}}{\partial y} + \frac{D_{\widehat{T}}}{\widehat{T}_\infty}\left(\frac{\partial\widehat{T}}{\partial y}\right)^2\right\} \tag{10}$$

.

The implementation of suitable similarity transformations is as follows:

$$\eta = y(a/\upsilon_f)^{1/2},\ \widehat{u} = axf',\widehat{v} = -(a/\upsilon_f)^{1/2}f,\ \theta = \frac{\widehat{T}-\widehat{T}_\infty}{\widehat{T}_w-\widehat{T}_\infty},\ \chi = \frac{\widehat{C}-\widehat{C}_\infty}{\widehat{C}_w-\widehat{C}_\infty} \tag{11}$$

.

The following are the features of hybrid nanofluids integrating nanoparticles: density, heat capacity, thermal conductivity, and dynamic viscosity ref ([40]).

$$\mu_{nf} = \mu_f\Big/(1-\phi_1)^{2.5}, \\ \rho_{nf} = (1-\phi)\rho_f + \phi\rho_s, \\ (\rho Cp)_{nf} = (1-\phi)(\rho Cp)_f + \phi(\rho Cp)_s \tag{12}$$

.

Upon the utilization of the similarities stated in the Eq. (11), the Eqs. (4–9) and (10) are reduced to as follows:

$$\frac{f'''}{A_1A_2}\left(\left\{1+\frac{1}{\beta}\right\} + \left\{1+We^2f''^2\right\}^{(m-3)/2}\left\{1+mWe^2f''^2\right\}\right) \\ +f''f - f'^2 - \frac{1}{A_1A_2}Kf' = 0, \tag{13}$$

$$\frac{A_3}{\Pr}\left\{1-\frac{8R}{3}\right\}\theta'' + \frac{4R}{\Pr(\theta_p-1)}\frac{d^2}{d\eta^2}\left(1+(\theta_p-1)\theta\right)^2 + f\theta' + A_4\left(Nb\theta'\chi' + Nt\theta'^2\right) = 0, \tag{14}$$

$$\chi'' + Le\Pr(f\chi' - K_c\chi) + \frac{Nt}{Nb}\theta'' = 0. \tag{15}$$

and

$$f(0) = 0, f'(0) = 1 + \left(1+\frac{1}{\beta}\right)(\gamma f''(0) + \delta f'''(0)), \theta(0) = 1, \chi(0) = 1 \tag{16}$$

$$f'(\infty)\to\infty, \theta(\infty)\to 0, \chi(\infty)\to 0 \tag{17}$$

.

where,

$We = \Gamma a\mathrm{Re}_x^{1/2}$ - Weissenberg number,	$K = \frac{\upsilon_f}{ak^*}$ - Porosity parameter,
$\Pr = \frac{\upsilon_f(\rho Cp)_f}{k_f}$ Prandtl number,	$R = \frac{4\sigma^*\widehat{T}_\infty^3}{k_f\alpha^*}$ - Radiation parameter
$\theta_p = \frac{\widehat{T}_w}{\widehat{T}_\infty}$ - Temperature ratio,	$Nb = \frac{\tau D_B(\widehat{C}_w-\widehat{C}_\infty)}{\upsilon_f}$ - Brownian motion parameter,
$Nt = \frac{\tau D_{\widehat{T}}(\widehat{T}_w-\widehat{T}_\infty)}{\upsilon_f\widehat{T}_\infty}$ Thermophoresis parameter,	$Le = \frac{\alpha_f}{D_B}$ - Lewis number,
$K_c = \frac{K_r^*}{a}$ - chemical reaction parameter,	$\gamma = A\sqrt{\frac{a}{\upsilon_f}}(\gamma > 0)$ - First order slip parameter
$\delta = \frac{Ba}{\upsilon_f}(\delta > 0)$ - Second order slip parameter,	A_1, A_2, A_3, A_4 - Constants

.

The Engineering factors with their reduced form are given as follows:

$$Cf = \frac{\tau_w|_{y=0}}{\rho_f u_w^2},\quad \tau_w = \mu_{nf}\left(\frac{\partial u}{\partial y}\right)\left\{\left(1+\frac{1}{\beta}\right) + \left(1+\Gamma^2\left(\frac{\partial u}{\partial y}\right)^2\right)^{\frac{m-1}{2}}\right\}, \tag{18}$$

$$\mathrm{Re}^{1/2}Cf = \frac{1}{A_1}f''(0)\left\{\left(1+\frac{1}{\beta}\right) + \left[1+\mathrm{We}^2f''^2(0)\right]\right\}$$

$$Nu = \frac{q_w}{k_f\Delta T},\ q_w = -k_{nf}\frac{\partial T}{\partial y}\Big|_{y=0} + q_r|_{y=0} \\ \mathrm{Re}^{-1/2}Nu = -\theta'(0)\left[\frac{k_{nf}}{k_f} + \frac{4R}{3}\left\{(\theta_p-1)\theta - 1\right\}\right] \tag{19}$$

$$Sh = \frac{-x}{\Delta C}\left(\frac{\partial C}{\partial y}\right)_{y=0},\ q_m = -D\left(\frac{\partial C}{\partial y}\right)_{y=0} \to \mathrm{Re}^{-1/2}Sh = -\chi'(0). \tag{20}$$

.

3. Methodology

This section covers the techniques used to derive solutions as well as code validation. Initially appeared as PDEs are translated into ODEs with

similarity variables and then bvp−4c [41] is used to compute the solution for Eq. 13−17. Some basic assumptions are made while calculating the model's solution, we turn the modified equations into a first-order system by inserting novel parameters. These additional parameters are replaced as follows:

$$\left\{\begin{array}{l} f=\Theta_1, \\ f'=\Theta_2, \\ f''=\Theta_3, \\ \theta=\Theta_4, \\ \theta'=\Theta_5, \\ \chi=\Theta_6, \\ \chi'=\Theta_7 \end{array}\right\} \tag{21}$$

$$\Theta_3' = -\frac{A_1A_2}{\left[\left(1+\beta^{-1}\right)+\left\{1+\mathrm{We}^2{\Theta_3}^2\right\}^{\frac{m-3}{2}}\left\{1+\eta\mathrm{We}^2{\Theta_3}^2\right\}\right]}\left(+\Theta_3\Theta_1-{\Theta_2}^2-\frac{1}{A_1A_2}K\Theta_2\right), \tag{22}$$

$$\Theta_4' = \frac{-1}{\frac{A_3}{\mathrm{Pr}}\left(1-\frac{8R}{3}\right)}\left(\frac{4R}{\mathrm{Pr}(\theta_p-1)}\frac{d^2}{d\eta^2}\left[1+(\theta_p-1)\Theta_4\right]^2 + \Theta_1\Theta_5+A_4\left(Nb\Theta_5\Theta_7+Nt{\Theta_7}^2\right)\right), \tag{23}$$

$$\chi'' = -\left(LePr(\Theta_1\Theta_7-K_c\Theta_6)+\frac{Nt}{Nb}\Theta_4'\right). \tag{24}$$

and

$$\Theta_1(0)=0, \Theta_2(0)=1+\left(1+\beta^{-1}\right)\left[\gamma\Theta_3(0)+\delta\Theta_1\Theta_3'(0)\right], \Theta_4(0)=1, \Theta_6(0)=1, \Theta_2(\infty)\to\infty, \infty\,\Theta_4(\infty)\to 0, \Theta_6(\infty)\to 0 \tag{25}$$

.

Initially, the Eqs. (22) to (24) entered into the bvp−4c solver. bvp−4c yields the component called "sol". The "sol" component consists of a few functions, with the syntax as follows: "sol = bvp4c (@odebvp, ode, solinit)". The "@odebc" function aids in defining the boundary conditions (25). For encoding the initial mesh points, as well as the primary solution approximation the "solinit" function is utilized. The solver will then execute, involving the replacement of the parameters specified follows: $We = 1.2$, $\delta = -0.2$, $\gamma = 0.2$, $\theta_p = 0.5$, $K_c = 1.0$, $m = 1.0$, $Le = 2.0$, $Nt = 1.2$, $Nb = 1.2$, $R = 1.5$, $\beta = 1.3$, and $K = 0.5$ with properties of nanoparticles and base fluid itemized in Table 2. Besides, after the numerical results were compared with the findings of earlier investigations (see Table 3), they were remarkably similar.

4. Results and discussion

The following section illustrates the solutions obtained from numerical methodology and expressed with multiple graphs. This discussion mainly focuses on the influence of various parameters, like Thermophoresis and Brownian motion (Nt, Nb), porosity and Casson

Table 2
Thermophysical properties of nanofluid and base fluid see [42,43].

Particles	$\rho(kgm^{-3})$	$Cp(Jkg^{-1}K^{-1})$	$k(Wm^{-1}K^{-1})$
Sodium Alginate	989	4175	0.6376
GO	1800	717	5000

Table 3
Results of the Nusselt number *Nu* for variations of Pr with $R = \theta_p = Nb = Nt = 0$ in the absence of A_3 and A_4.

Pr	Previous results [34]	Current study
0.72	0.7987	0.7981
1.0	1.0000	1.0000
3.0	1.9235	1.9229
7.0	3.0731	3.0735
10	3.7205	3.7202

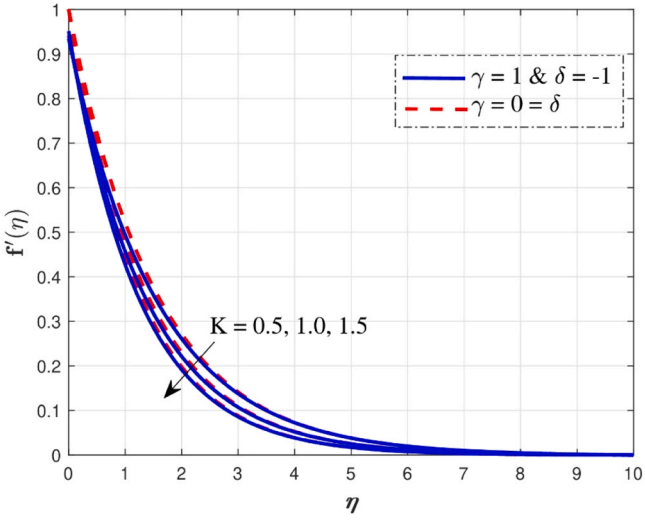


Fig. 4. Effect of K over $f'(\eta)$.

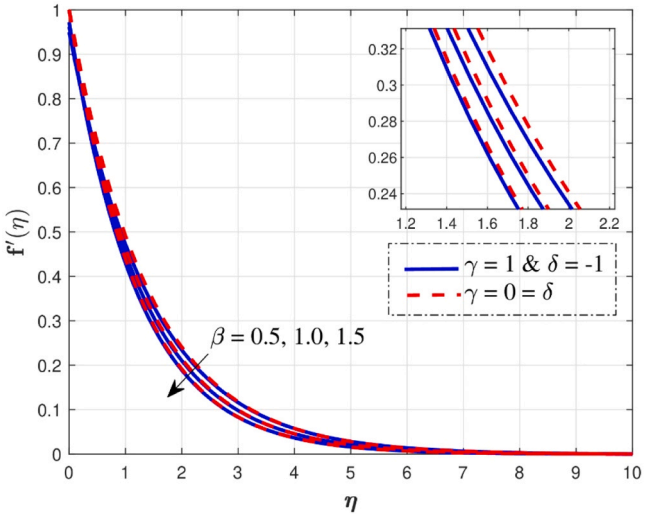


Fig. 5. Effect of β over $f'(\eta)$.

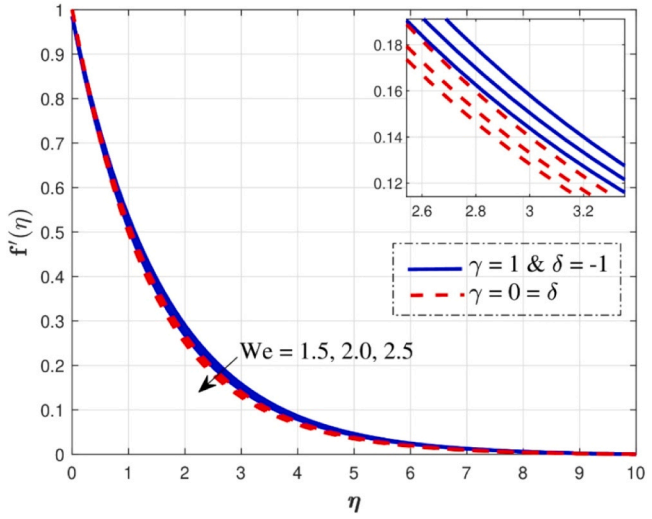


Fig. 6. Influence of *We* on $f'(\eta)$.

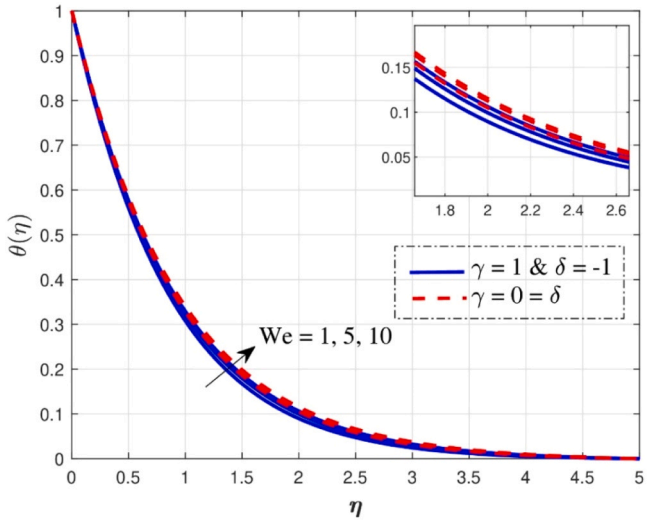


Fig. 7. Influence of *We* on $\theta(\eta)$.

parameters (K, β), Weissenberg and Lewis number (We, Le), and Quadratic radiation parameter R over respective profiles, such as momentum $f'(\eta)$, temperature $\theta(\eta)$, and concentration $\chi(\eta)$. The authors assessed the model in two scenarios: with slip and without slip conditions. Solid blue line curves on the graphs indicate solutions for slip conditions, whereas dotted line curves represent solutions without slip conditions.

Fig. 4 depicts the nature of $f'(\eta)$ for varying values of parameter K. It seems that fluid velocity gets reduced for rising values of K. Physically, the growth of porosity leads to lower permeability, causing significant resistance to fluid flow rate, hence reducing fluid velocity. It is seen that the reduction is more in the presence of slip conditions. A similar nature is witnessed in $f'(\eta)$ for increasing the value of β in Fig. 5. It is because the augmentation of β suggests that the fluid's non-Newtonian behaviour is greater. This enhanced non-Newtonian nature produces stronger viscous forces within the fluid, which hinder the fluid motion and lower the thickness of the boundary layer. The slip effect gets more significant as the Casson parameter value increases. Also, its presence at the boundary contributes to the drop in fluid velocity.

The effect of We on $f'(\eta)$ and $\theta(\eta)$ is displayed in Fig. 6 and Fig. 7. The decreasing trend is witnessed in $f'(\eta)$. This is because the higher the Weissenberg number, the greater the fluid's non-Newtonian, viscoelastic

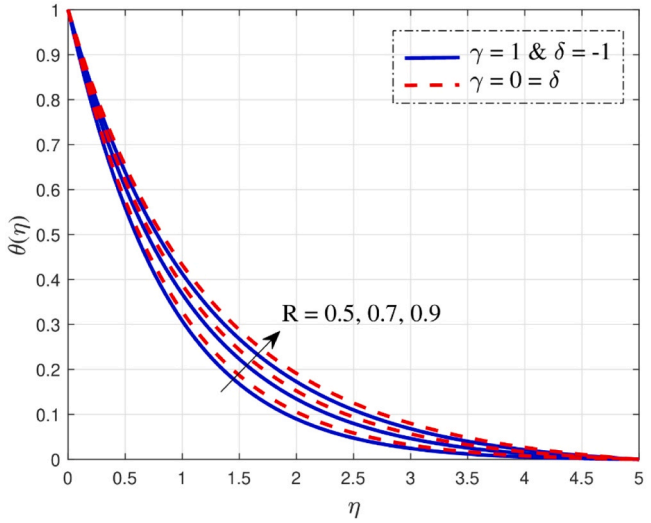


Fig. 8. Radiation impact on thermal field $\theta(\eta)$.

behaviour. This greater viscoelastic nature induces greater internal stresses in the fluid, slowing the fluid's velocity. In the absence of the slip condition effect, the fluid velocity drops due to the formation of a boundary layer along the solid layer where the no-slip condition is in effect, resulting in a decrease in fluid velocity when compared to the free-stream velocity away from the boundary.

But Fig. 7 portrays the opposite trend in $\theta(\eta)$, where an increase in $\theta(\eta)$ is obtained for rising We values. Physically, as the Weissenberg number grows, elastic effects become more important than viscous effects, resulting in rapid heat dissipation. This dissipative heating phenomenon raises the fluid's temperature, which is more prominent at higher Weissenberg numbers when elastic effects dominate. The increase is more prominent in the case of the no-slip condition.

Fig. 8 is drawn out to analyse the increasing behaviour of $\theta(\eta)$ for growing values of R. From a physical point of view, the growing radiative flux from quadratic radiation serves as a volumetric heat source in the energy equation. This additional thermal energy input is dispersed and redistributed, resulting in a total rise in thermal fields across the participating medium as the radiation effects build up. This raises temperatures over the thermal field. The influence of Nb over $\theta(\eta)$ is illustrated in Fig. 9. It is seen that on increasing Nb, curves of $\theta(\eta)$ raises. From a physical standpoint, Brownian motion causes random

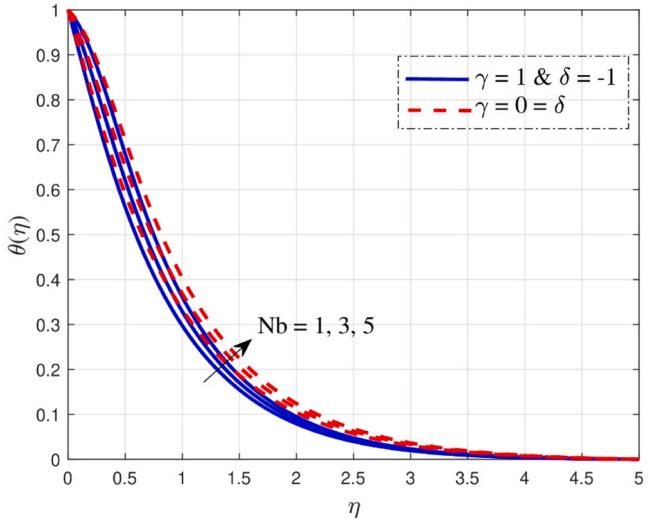


Fig. 9. Effect of Nb over $\theta(\eta)$.

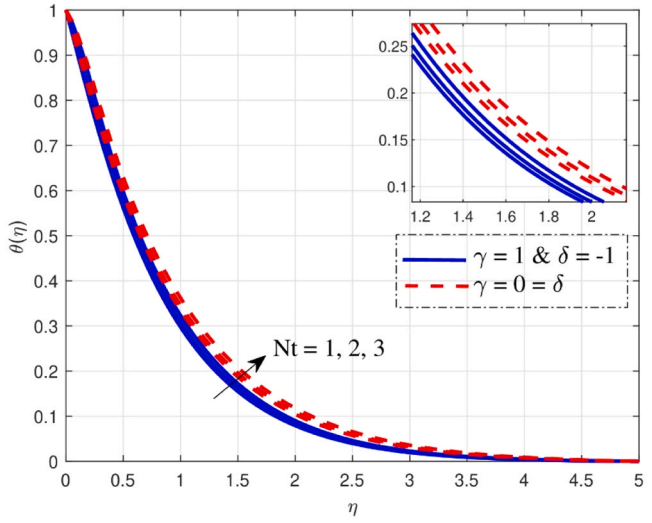


Fig. 10. Variation in $\theta(\eta)$ curves for several values of *Nt*.

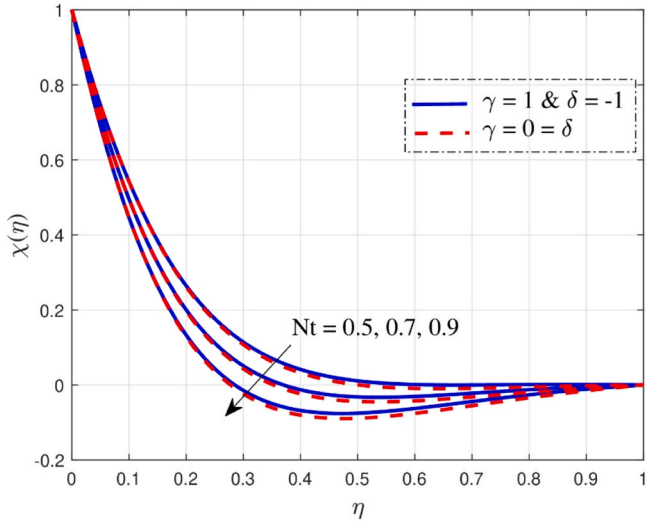


Fig. 11. Variation in $\chi(\eta)$ curves for *Nt* values.

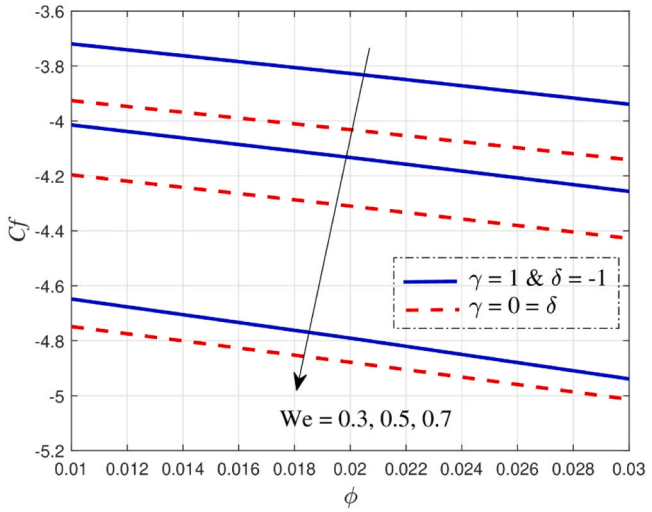


Fig. 12. Change in the nature of *Cf* for distinct values of *We*.

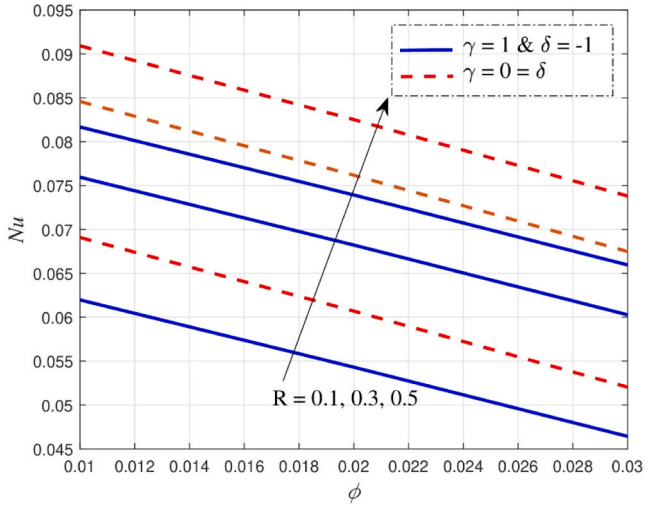


Fig. 13. Change in the nature of *Nu* for distinct values of *R*.

nanoparticle transportation, which contributes to the rising temperatures of the fluid in the boundary layer and causes an overall rise in the thermal field. Moreover, the more restricted no-slip condition constrains heat dissipation techniques such as advection and diffusion in addition additionally triggering viscous heating effects, driving temperatures to rise faster than in slip flow conditions in both Figs. 8 and 9.

The increase of $\theta(\eta)$ for growing values of *Nt* values is documented in Fig. 10. Stronger thermophoretic displays particle redistribution of highly conductive nanoparticles from cold to hot places and functions as a volumetric heat source in hotter zones. This has an impact on the growth of the thermal boundary layer, generally increasing its thickness and hence escalating temperatures. Further, the no-slip condition also facilitates the upsurge in the thermal field $\theta(\eta)$.

Fig. 11 presents the variation caused in $\chi(\eta)$ for varying values of *Nt*. It is observed that curves of $\chi(\eta)$ decreases for uplifting the parametric values of *Nt*. This is because, the raised thermophoresis effect induces suspended particles to disperse away from specific areas, resulting in a drop in overall concentration distribution. Furthermore, the no-slip condition, which does not include surfactants, will result in a higher drop in the concentration profile than slip conditions.

The change in the nature of *Cf* for diverse values of *We* is portrayed in Fig. 12. It is witnessed *Cf* escalates when Weis raised. Physically, when a viscoelastic fluid flows through a surface, the fluid molecules' elastic characteristics compel them to stretch and travel along flow path. This extending and orientation of the molecules can reduce the effective viscosity of the fluid at the solid barrier producing less shear stress or skin friction on the surface. From figure is can observed that the impact is significant more in case of no-slip condition. This drags reduction behavior has practical significance in a variety of sectors, including the transfer of crude oil and other viscoelastic fluids via pipelines or any other surfaces, where minimizing skin friction may result in considerable reductions in energy consumption and greater flow efficiency.

Fig. 13 shows the behaviour of *Nu* caused by escalating the values of *R*. There is a spike in the *Nu* curves. This is due to the fact that when the radiation strength goes up, correspondingly rises the radiative heat flux over the boundary. This excess radiative heat transfer enhances the total heat transfer rate, which used to be driven by conduction and convection. The no-slip condition allows for the formation of a thermal boundary layer near the solid surface. This thermal boundary layer promotes the transmission of heat from solid to fluid or vice versa, resulting in increased convective heat transfer rates and thus the Nusselt number. Engineers may increase the overall performance and endurance of solar aircraft by researching the Nusselt number and its implications for heat transfer.

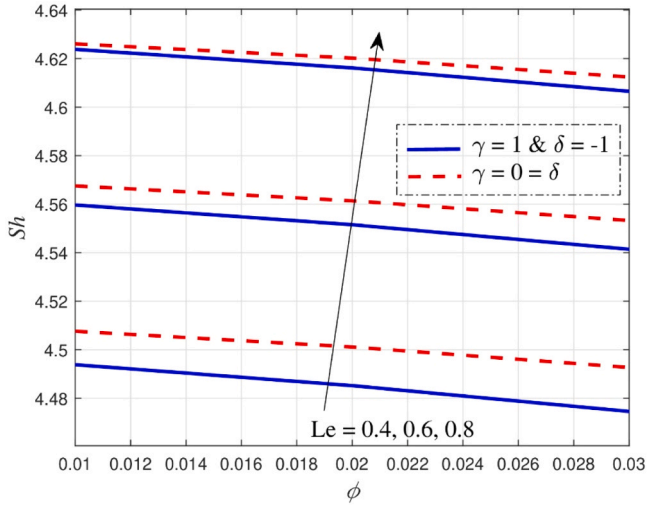


Fig. 14. Behavior of *Sh* upon the impact of *Le*.

The influence of *Le* over *Sh* is analyzed in the Fig. 14. On escalating the *Le* values, an upsurge in mass transfer is found. It is because, a higher *Le* can lead to a slimmer thermal boundary layer than the concentration boundary layer. This might lead to deeper concentration gradients at the surface, boosting the convective mass transfer rate and, thus, the Sherwood number is enhanced. The no-slip condition causes the growth of a concentration boundary layer near to the solid surface, in which the concentration of the species in the fluid ranges from surface to free-stream concentration.

This concentration boundary layer empowers movements of the species to from the solid to the fluid or vice versa, resulting in enhanced convective mass transfer rates. The Sherwood number is a critical metric for measuring mass transfer rates in applications such as drying, cooling via evaporation, and chemical vapor deposition. Fig. 15 displays the streamline pattern for Carreau-Casson fluid in the presence and absence of β.

Table 4 shows the quantitative analysis of friction, heat and mass transfer rates under the influence of parameters (β, *We*, *K*, *R*, *Nb*, *Nt*). From table, it can be observed that *We* and β reduces *Cf*%, keeping effect on heat and mass transfer rates minimal. Augmented values of *K* increases *Cf*% which showcases significant resistance from porous effect. Next, growing values of *R* minimizes *Nu*%and *Sh*% indicating suppression in both heat and mass transfer rates. Further, raise in both *Nb* and *Nt* improves both *Nu*%and *Sh*% demonstrating migration of nanoparticles enhancing thermal and species transfer. The outcomes from this analysis are useful in studying cooling systems, heat exchange devices, and in chemical labourites where heat and mass transfer is managed.

5. Conclusions

In this study, the nature of Carreau-Casson nanofluid flow across stretching sheet is examined. The governing PDE model was reduced to ODE model and solved via bvp−4c technique. The study has been analysed in two different cases: slip and no-slip conditions. The quantitative results study has been conducted between engineering factors and parameters for study of friction, heat and mass transfer rates. The key outcomes put forth as follows:

- The velocity of the nanofluid declines for both porosity parameter and Casson parameter. the reduction is more in the presence of slip condition.
- It was found that when Weissenberg number is elevated it results in hindering flow velocity whereas opposite trend is witnessed in case of thermal field.

Table 4
Quantitative analysis of *Cf*%, *Nu*%, and *Sh*%.

Parameters	Scales	*Cf*%	*Nu*%	*Sh*%
β	0.5	7.60	0.12	−0.10
	0.7	7.41	0.08	−0.14
	0.9	7.24	0.06	−0.16
We	1.3	7.59	0.12	−0.10
	1.5	7.56	0.12	−0.10
	1.7	7.53	0.12	−0.10
K	0.5	7.60	0.12	−0.10
	0.6	7.72	−0.10	−0.11
	0.7	7.84	0.13	−0.10
R	1.5	7.60	0.12	−0.10
	1.7	7.60	−0.03	−0.16
	1.9	7.60	−0.17	−0.24
Nb	1	7.60	0.12	−0.10
	3	7.60	3.45	0.84
	5	7.60	7.56	1.30
Nt	1	7.60	0.12	−0.10
	1.5	7.60	1.19	0.41
	2	7.60	2.36	0.96

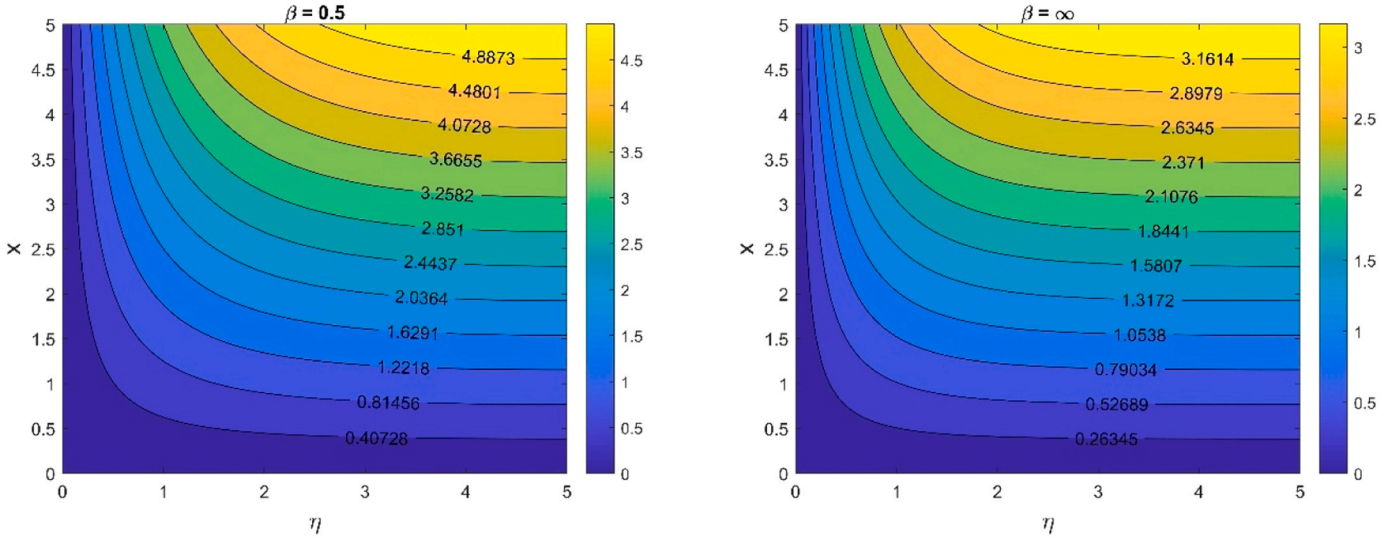


Fig. 15. Streamline pattern for Carreau-Casson fluid in the presence and absence of β.

- Thermal characteristics for nanofluid flow are enhanced for larger values of radiation parameter in both slip conditions.
- Increased values of Thermophoresis and Brownian motion lead to a rise in the thermal field.
- Upsurge in the thermophoresis parameter cause concentration profile to decline and the drop is significant in the case of a no-slip condition.
- The skin friction is reduced for larger values of Weissenberg number. Moreover, the decrease is more in the no-slip case.
- For larger values of radiation, an enhanced convective heat transfer is observed.
- A rise in the convective mass transfer rate is seen for bigger values of Lewis number in the existence of a no-slip case.
- From quantitative analysis, we witnessed low skin friction for higher Weissenberg number and casson parameter but it increases for porosity parameter. On the other hand, raise in Thermophoresis and Brownian motion greatly improves heat and mass transfer rates. Also, increasing radiation parameter lowers both heat and mass transfer rates.

Future work

The study focused on graphene oxide nanoparticles, but future research could look into other nanoparticle materials such as carbon nanotubes, metal oxides, or hybrid nanoparticles to improve Carreau-Casson nanofluid performance in boundary layer flows by improving thermal conductivity, rheological properties, and drag reduction. Alternative non-Newtonian fluid models, such as the power-law, Bingham plastic, and Herschel-Bulkley models, could be further investigated to reflect the fluid's rheological characteristics better and provide more insight into drag reduction techniques. Optimizing nanoparticle concentration using parametric research or optimization approaches might balance drag reduction, heat transfer, and mass transfer performance.

The current work is focused on a stretched surface, which can be studied further by expanding studies to other flow geometries essential to solar aircraft, such as airfoils, wings, and heat exchangers, which would give a broader understanding of the fluid's behavior and possibilities for drag reduction and thermal management.

CRediT authorship contribution statement

Mukannan Arivanandhan: Writing – review & editing, Visualization, Supervision, Conceptualization. **Gadigeppa Myacher Sachin:** Writing – original draft, Methodology, Formal analysis. **Ulavathi Shettar Mahabaleshwar:** Writing – review & editing, Supervision, Methodology, Formal analysis, Conceptualization. **Chan Andy:** Writing – review & editing, Supervision, Methodology, Formal analysis, Conceptualization. **Kandavkovi Mallikarjuna Nihaal:** Writing – original draft, Validation, Software, Methodology, Formal analysis. **Laura Milena Pérez:** Writing – review & editing, Visualization, Supervision, Software, Conceptualization.

Declaration of Competing Interest

The authors declare that they have no known competing financial interests or personal relationships that could have appeared to influence the work reported in this paper.

Acknowledgements

L.M.P. acknowledges partial financial support from ANID through FONDECYT 1240985 and from the Centers of Excellence with BASAL/ANID CIA250002, CEDENNA.

Data availability

The datasets generated and/or analyzed during the current study are available from the corresponding author upon reasonable request.

References

[1] S.U.S. Choi, J. Eastman, Enhancing thermal conductivity of fluids with nanoparticles 66 (1995).
[2] J. Buongiorno, Convective transport in nanofluids, J. Heat. Transf. 128 (Mar. 2006) 240–250, https://doi.org/10.1115/1.2150834.
[3] F. Waseem, M. Sohail, N. Sarhan, E.M. Awwad, M.J. Khan, Utilization of OHAM to investigate entropy generation with a temperature-dependent thermal conductivity model in hybrid nanofluid using the radiation phenomenon, Open. Phys. 22 (1) (Jan. 2024), https://doi.org/10.1515/phys-2024-0059.
[4] K.V. Modi, P.R. Patel, S.K. Patel, Applicability of mono-nanofluid and hybrid-nanofluid as a technique to improve the performance of solar still: a critical review, J. Clean. Prod. 387 (Feb. 2023) 135875, https://doi.org/10.1016/j.jclepro.2023.135875.
[5] U.S. Mahabaleshwar, M. Rudraiah, H. Huang, B.A. Sunden, An impact of ternary nanofluid on a micropolar fluid with inclined MHD, slip flow and heat transfer, Int. J. Numer. Methods Heat. Fluid. Flow. 34 (5) (Mar. 2024) 2065–2093, https://doi.org/10.1108/HFF-07-2023-0384.
[6] M. Ijaz Khan, A. Kumar, T. Hayat, M. Waqas, R. Singh, Entropy generation in flow of Carreau nanofluid, J. Mol. Liq. 278 (Mar. 2019) 677–687, https://doi.org/10.1016/j.molliq.2018.12.109.
[7] P. Santoshi, V. Gurrampati, P. Padma, Numerical scrutinization of three dimensional casson- carreau nano fluid flow, pp. xx–xx, J. Appl. Comput. Mech. 6 (Jul. 2020), https://doi.org/10.22055/JACM.2019.29377.1593.
[8] S. Li, F. Ali, A. Zaib, L. Karuppusamy, S. Eldin, M. Khan, Bioconvection effect in the Carreau nanofluid with Cattaneo–Christov heat flux using stagnation point flow in the entropy generation: Micromachines level study, Open. Phys. 21 (Mar. 2023), https://doi.org/10.1515/phys-2022-0228.
[9] K. Ramesh, F. Mebarek-Oudina, A.I. Ismail, B.R. Jaiswal, A. Warke, R.K. Lodhi, Computational analysis on radiative non-Newtonian Carreau nanofluid flow in a microchannel under the magnetic properties, Sci. Iran. 30 (Apr. 2023) 376–390, https://doi.org/10.24200/SCI.2022.58629.5822.
[10] H.A. Madkhali, M. Nawaz, S. Rana, S.O. Alharbi, A.S. El-Shafay, Mohamed R. Ali, A.S. Hendy, Effect of Cattaneo-Christov heat and mass flux in Carreau-Yasuda tri-nanofluid, Case Stud. Therm. Eng. 53 (Jan. 2024) 103787, https://doi.org/10.1016/j.csite.2023.103787.
[11] S. Bilal, I.A. Shah, M. Rashid, I. Khan, Impact of activation energy on carreau nanofluid flow over non-linear stretching surface, Heliyon 10 (1) (Jan. 2024) e23934, https://doi.org/10.1016/j.heliyon.2023.e23934.
[12] A. Manigandan, D.H. Babu, B. Venkateswarlu, P.V. Satya Narayana, A. Misra, M. K. Nayak, G. Sarojamma, Comparative analysis of heat transfer in hybrid nanofluid flow over an exponentially stretching sheet with variable fluid properties, J. Therm. Anal. Calorim. 151 (1) (Jan. 2026) 701–717, https://doi.org/10.1007/s10973-025-14849-7.
[13] K.M. Nihaal, U.S. Mahabaleshwar, L.M. Pérez, P. Cattani, An Impact of Induced Magnetic and Cattaneo-Christov Heat Flux Model on Nanofluid Flow across a Stretching Sheet, J. Appl. Comput. Mech. (2024), https://doi.org/10.22055/jacm.2024.45421.4365.
[14] F. Gamaoun, Z. Ullah, N. Ameer Ahammad, B.M. Fadhl, B.M. Makhdoum, A. Abbas Khan, Effects of thermal radiation and variable density of nanofluid heat transfer along a stretching sheet by using Keller Box approach under magnetic field, Therm. Sci. Eng. Prog. 41 (Jun. 2023) 101815, https://doi.org/10.1016/j.tsep.2023.101815.
[15] M.A. Al Zubi, M. Naveed Khan, N. Ahsan, M. Hussien, K.A. Gepreel, M.D. Albalwi, Numerical heat transfer analysis of bio convective flow of non-Newtonian nanofluid with Darcy-Forchheimer effect over a curved stretching surface, Numer. Heat. Transf. Part. Appl. 87 (1) (Jul. 2024) 2373967, https://doi.org/10.1080/10407782.2024.2373967.
[16] F. Waseem, M. Sohail, S.A. Lone, G. Chambashi, Numerical simulations of heat generation, thermal radiation and thermal transport in water-based nanoparticles: OHAM study, Sci. Rep. 13 (1) (Sep. 2023) 15650, https://doi.org/10.1038/s41598-023-42582-4.
[17] A. Ahmed, M.N. Khan, A. Alhowaity, H.F. Alrihieli, N.S. Khashi'ie, Finite-speed thermal transport and Lorentz force effects in buoyant convective flow: a Cattaneo–Christov approach, J. Eng. Res. (May 2026), https://doi.org/10.1016/j.jer.2026.05.006.
[18] H. Upreti, P. Bartwal, A.K. Pandey, O.D. Makinde, Heat transfer assessment for Au-blood nanofluid flow in Darcy-Forchheimer porous medium using induced magnetic field and Cattaneo-Christov model, Numer. Heat. Transf. Part. B Fundam. 84 (4) (Oct. 2023) 415–431, https://doi.org/10.1080/10407790.2023.2209281.
[19] U.S. Mahabaleshwar, T. Anusha, M. Hatami, Analysis of a Stagnation Point Flow with Hybrid Nanoparticles over a Porous Medium, Fluid. Dyn. Mater. Process. 19 (2) (2023), https://doi.org/10.32604/fdmp.2022.022002.
[20] S.T. Abbas, S. Jahan, A. Afzal, M. Sohail, Bio-Convective Thermally Radiated Casson Fluid Model PDEs Past over a Darcy-Forchheimer Porous Stretched Sheet via OHAM Strategy (Trans.), Babylon. J. Math. 2024 (2024) 56–72, https://doi.org/10.58496/BJM/2024/008.
[21] F. Waseem, M. Sohail, A. Singh, Entropy analysis of three-dimensional stretched magnetized hybrid nanofluid with thermal radiation and heat generation,

BioNanoScience 14 (2) (Jun. 2024) 547–565, https://doi.org/10.1007/s12668-023-01267-y.
[22] M. Sohail, F. Waseem, K. Abodayeh, E. Rafique, Analysis of entropy generation on Darcy-Forchheimer squeezed hybrid nanofluid flow between two parallel rotating disks by considering thermal radiation and viscous dissipation, Numer. Heat. Transf. Part. B Fundam. 87 (1) (Mar. 2025) 2391501, https://doi.org/10.1080/10407790.2024.2391501.
[23] K. Thriveni, B. Mahanthesh, Significance of variable fluid properties on hybrid nanoliquid flow in a micro-annulus with quadratic convection and quadratic thermal radiation: Response surface methodology, Int. Commun. Heat. Mass. Transf. 124 (May 2021) 105264, https://doi.org/10.1016/j.icheatmasstransfer.2021.105264.
[24] P. Rana, A. Kumar, Nonlinear buoyancy driven flow of hybrid nanoliquid past a spinning cylinder with quadratic thermal radiation, Int. Commun. Heat. Mass. Transf. 139 (Dec. 2022) 106439, https://doi.org/10.1016/j.icheatmasstransfer.2022.106439.
[25] L.Y. Jiann, A.Q. Mohamad, N.A. Rawi, D.L. Chaun Ching, N.A. Mohd Zin, S. Shafie, Thermal analysis of melting effect on Carreau fluid flow around a stretchable cylinder with quadratic radiation, Propuls. Power Res. 13 (1) (Mar. 2024) 132–143, https://doi.org/10.1016/j.jppr.2024.02.006.
[26] E.M. Elsaid, M.R. Eid, M. Abd El-Haleem, Kh Lotfy, G.R. Elnaggar, S.A. Hussein, Comprehensive modeling and thermal control of selenium nanoparticle enhanced blood flow under biomagnetic and ferrohydrodynamic effects with quadratic thermal radiation, Int. J. Numer. Methods Heat. Fluid. Flow. (May 2026) 1–27, https://doi.org/10.1108/HFF-02-2026-0134.
[27] G. Mandal, P. Kaswan, A. Sarkar, M. Kezzar, Enhanced heat transfer characteristics of Casson–Williamson trihybrid nanofluid under quadratic thermal radiation over a porous stretching surface, Int. J. Numer. Methods Heat. Fluid. Flow. (Apr. 2026) 1–35, https://doi.org/10.1108/HFF-01-2026-0055.
[28] S. Abbas, M. Sohail, Entropy Analysis for Three-Dimensional Stretched Flow of Viscous Fluid Engaging Radiation Effect and Double Diffusion Phenomenon (vol.), Int. J. Emerg. Multidiscip. Math. 3 (May 2024), https://doi.org/10.59790/2790-3257.1047.
[29] S. Hazarika, S. Ahmed, Brownian motion and thermophoresis behavior on micro-polar nano-fluid—A numerical outlook, Math. Comput. Simul. 192 (Feb.2022) 452–463, https://doi.org/10.1016/j.matcom.2021.09.012.
[30] K. Sudarmozhi, D. Iranian, N. Alessa, Investigation of melting heat effect on fluid flow with brownian motion/thermophoresis effects in the occurrence of energy on a stretching sheet, Alex. Eng. J. 94 (May 2024) 366–376, https://doi.org/10.1016/j.aej.2024.03.065.
[31] S.A. Agunbiade, A.A. Ayoade, T.L. Oyekunle, M.T. Akolade, Brownian motion and thermophoresis influence in magnetized Maxwell upper-convected stagnation point fluid flow via a stretching porous surface, J. Taibah Univ. Sci. 18 (1) (Dec. 2024) 2301130, https://doi.org/10.1080/16583655.2023.2301130.
[32] F. Ali, A. Zaib, S. Reddy, M.H. Alshehri, N.A. Shah, Impact of thermal radiative Carreau ternary hybrid nanofluid dynamics in solar aircraft with entropy generation: significance of energy in solar aircraft, J. Therm. Anal. Calorim. 149 (4) (Feb. 2024) 495–1513, https://doi.org/10.1007/s10973-023-12734-9.
[33] M. Ramzan, M. Javed, S. Rehman, D. Ahmed, A. Saeed, P. Kumam, Computational Assessment of Microrotation and Buoyancy Effects on the Stagnation Point Flow of Carreau–Yasuda Hybrid Nanofluid with Chemical Reaction Past a Convectively Heated Riga Plate, ACS Omega 7 (34) (Aug. 2022) 30297–30312, https://doi.org/10.1021/acsomega.2c03570.
[34] K. Jyothi, P. Sudarsana Reddy, M. Suryanarayana Reddy, Carreau nanofluid heat and mass transfer flow through wedge with slip conditions and nonlinear thermal radiation, J. Braz. Soc. Mech. Sci. Eng. 41 (10) (Oct. 2019) 415, https://doi.org/10.1007/s40430-019-1904-7.
[35] S. Mukhopadhyay, P.R. De, K. Bhattacharyya, G.C. Layek, Casson fluid flow over an unsteady stretching surface, Ain Shams Eng. J. 4 (4) (Dec. 2013) 933–938, https://doi.org/10.1016/j.asej.2013.04.004.
[36] W. Al-Kouz, B. Mahanthesh, M.S. Alqarni, K. Thriveni, A study of quadratic thermal radiation and quadratic convection on viscoelastic material flow with two different heat source modulations, Int. Commun. Heat. Mass. Transf. 126 (Jul. 2021) 105364, https://doi.org/10.1016/j.icheatmasstransfer.2021.105364.
[37] M. Arshad, A. Hussain, A. Hassan, Q. Haider, A.H. Ibrahim, M.S. Alqurashi, A. H. Almaliki, A. Abdussattar, Thermophoresis and brownian effect for chemically reacting magneto-hydrodynamic nanofluid flow across an exponentially stretching sheet, Energies 15 (1) (2022) 143, https://doi.org/10.3390/en15010143.
[38] Y.S. Daniel, Z.A. Aziz, Z. Ismail, F. Salah, Thermal radiation on unsteady electrical MHD flow of nanofluid over stretching sheet with chemical reaction, J. King Saud. Univ. - Sci. 31 (4) (Oct. 2019) 804–812, https://doi.org/10.1016/j.jksus.2017.10.002.
[39] N. Acharya, R. Bag, P.K. Kundu, Unsteady bioconvective squeezing flow with higher-order chemical reaction and second-order slip effects, Heat. Transf. 50 (6) (Sep.2021) 5538–5562, https://doi.org/10.1002/htj.22137.
[40] S.P.A. Devi, S.S.U. Devi, Numerical Investigation of Hydromagnetic Hybrid Cu –Al2O3 /Water Nanofluid Flow over a Permeable Stretching Sheet with Suction, Int. J. Nonlinear Sci. Numer. Simul. 17 (5) (Aug. 2016) 249–257, https://doi.org/10.1515/ijnsns-2016-0037.
[41] M.N. Khan, K. Choubani, S. Ahmad, H. Chen, M.A. Almeshaal, Numerical analysis of Soret and Dufour effects in chemically reactive bioconvective flow through a converging–diverging channel, Phys. Chem. Earth Parts ABC 144 (Oct. 2026) 104483, https://doi.org/10.1016/j.pce.2026.104483.
[42] U. Khan, A. Zaib, S.A. Bakar, S.K. Soid, A. Ishak, S. Elattar, A.M. Abed, Non-similar solutions of dissipative buoyancy flow and heat transfer induced by water-based graphene oxide nanofluid through a yawed cylinder, Lubricants 11 (2) (Feb. 2023) 60, https://doi.org/10.3390/lubricants11020060.
[43] M. Alghamdi, A. Wakif, T. Thumma, U. Khan, D. Baleanu, G. Rasool, Significance of variability in magnetic field strength and heat source on the radiative-convective motion of sodium alginate-based nanofluid within a Darcy-Brinkman porous structure bounded vertically by an irregular slender surface, Case Stud. Therm. Eng. 28 (Dec. 2021) 101428, https://doi.org/10.1016/j.csite.2021.101428.